Math. Model. Nat. Phenom. 17 (2022) 27
https://doi.org/10.1051/mmnp/2022030

Mathematical Modelling of Natural Phenomena
www.mmnp-journal.org

ON BEHAVIORAL RESPONSE OF CILIATED CERVICAL CANAL ON THE DEVELOPMENT OF ELECTROOSMOTIC FORCES IN SPERMATIC FLUID

Sara I. Abdelsalam[1,2,*] and A.Z. Zaher[3]

Abstract. The goal of this research is to conduct a theoretical investigation about the effect of the electroosmotic forces on the swimming of sperms throughout the cervical canal. To imitate male semen with self-propulsive spermatozoa, a hyperbolic tangent fluid is used as the base liquid. Swimming sperms move inside a ciliated cervical canal and peristalsis occurs due to the ciliated walls. The perturbation method is used to solve the controlling partial differential set of equations analytically. Due to self-propulsion of swimmers and long wavelength assumption, a creeping flow protocol is used throughout the stream. The stream pattern, velocity distribution, and pressure gradient (above and below the swimming sheet) solutions are produced and displayed with the relevant parameters. The outcomes of this manuscript show that the rheological parameters of hyperbolic tangent fluid are more appropriate to simulate and discuss the motility of cervical fluid. Moreover, the motility of mucus velocity is more applicable for small values of power law index n at the upper swimming sheet of propulsive spermatozoa. In addition, the mucus velocity increases in both region (upper and lower region of swimming sheet) with an increase of the electroosmotic parameter m_e and Helmholtz-Smoluchowski velocity U_{HS}. The present analysis provides a mathematical assessment to the swimmers' interaction through the ciliated genital tract where the embryo is affected by the interaction of ciliary activity.

Mathematics Subject Classification. 35Q35, 76W05, 37N25, 70E20.

Received March 24, 2022. Accepted June 28, 2022.

1. Introduction

Electroosmosis is the primary technique for detecting flow in a wide range of operations. This electroosmotic transfer is based on the fact that when a polar material is applied to an electrolyte framework, the electrolyte arrangement's reverse particles are allowed to migrate in direction of the charging interface, also referred to as the Stern sheet. In the domain of the charged sheet, an Electric Double Layer (EDL) is created and bound to an outer diffuse interface. When an exterior electrical field is supplied to the EDL, the particles in the EDL's dispersed region move to produce mass fluid displacement *via* the dense effect, which is commonly known as

Keywords and phrases: Electroosmotic forces, perturbation method, hyperbolic tangent fluid, swimming sperms transport, propulsive velocity, ciliated cervical canal.

[1] Instituto de Ciencias Matemáticas ICMAT, CSIC, UAM, UCM, UC3M, Madrid 28049, Spain.
[2] Basic Science, Faculty of Engineering, The British University in Egypt, Al-Shorouk City, Cairo 11837, Egypt.
[3] Basic Science, Faculty of Engineering, Shubra, Benha University, Cairo, Egypt.

* Corresponding author: sara.abdelsalam@bue.edu.eg

the electroosmotic flow (EOF). The electroosmosis principle governs the non-Newtonian fluid streams in bio-microfluidics applications. Non-Newtonian materials are common in manufacturing and engineering activities where a direct correlation between stress and deformation rate cannot be achieved. One of the most significant non-Newtonian systems designed for chemical engineering applications is the tangent hyperbolic fluid model since its rheological formulation is based upon liquid kinetic theory rather than analytical relationships [16]. Ramesh *et al.* [19] used the tangent hyperbolic fluid with nanoparticles (NPs) to numerically investigate the fluid properties under the effect of EOF. Their study through the porous medium showed that the electroosmotic parameter enhances the fluid flow. They further performed a comparison between the fluid properties with and without the electroosmosis where it was seen that the absence electroosmosis decelerates the flow whether it is Newtonian or non-Newtonian fluid. Jayavel *et al.* [11] analytically solved an electroosmotic fluid model combining nanoparticles and thermal effect on a tangent hyperbolic fluid through flexible boundaries. It was concluded that the electroosmotic parameter enhances the skin friction coefficient and increases the pressure gradient resistance uniformly. For more investigations about the impact of electroosmosis in combination with non-Newtonian fluid, reader may be referred to references [1, 13, 25].

Many scholars have conducted extensive studies on sperm delivery. These researchers were interested in determining the current state of knowledge about the movement of male sperm in the vagina through the bodily secretions that fill the vaginal waterway. The transmission of sperms through the cervix is regarded as significant research because it aids in the preservation of sperm integrity, which in turn influences human fertility and the survival of life. Cilia-generated propagation is essential in a wide range of physiological and cellular membranes. Cilia are protuberances that live on the outside of living cells. These are narrow projections of plasma membrane that are internally supported by cytoplasmic microtubules and measure around 1–10 μm in length. Abdelsalam *et al.* [2] studied the movement of sperms in the cervical conduit by taking the base fluid as the Eyring-Powell model simulating the sperms with self-propulsion propagation. Thanks to the electric field of research in the latter analysis, it was deduced that the electric field can control the movement of sperms inside the cervical conduit of the female reproductive system. Saleem and Munawar [21] studied the stream of a hyperbolic tangent model of fluid inside a channel lined with cilia which are distributed at equal intervals with magnetic field. It was then concluded that the size of bolus and pressure rise are increased with an increase in the length of cilia. Abdelsalam *et al.* [3] investigated the particle-fluid suspension of a non-Newtonian flow due to the propagation of cilia in a 2D channel. They found out that the bolus size is increased with an increase in the elliptic path of the cilia. Gaddum-Rosse [9] investigated the ciliary beat in the oviducts in two species *in vitro*. In 2005, Suarez and Pacey [22] researched the transportation of seminal fluid in the female reproductive duct where they confirmed that the detection of fertility problems may be significantly enhanced if more was understood about how sperm travels through the female reproductive canal and the processes that govern sperm migration. After that in 2016, Suarez [23] studied the selection of the fittest sperm by investigating the interaction of sperm with the reproductive duct in many ways allowing better migration to the sperm while keeping it alive. Few relevant studies are given in the references [4, 5, 12, 14, 27].

During sexual intercourse, spermatic fluid is injected inside within the vaginal canal through emission of semen at fast tempo rates (propulsatile ejaculation), and those that are not expelled beyond the vaginal canal are those that can access the cervix. The activity of this spermatozoa necessitates a certain PH level that is stabilized by the topmost vaginal and lasts for several minutes, allowing sufficient time for the sperms to move [2, 14]. Walait *et al.* [17] shed some light on the propulsive velocity of sperms where it was found that the propulsive velocity in the Newtonian model is higher than that of the couple stress model which acted as the cervical mucus. Radhakrishnamacharya and Sharma [26] regarded the Newtonian fluid model as the mucus because of its varying viscosity and they discovered that when the peripheral layer viscosity increases, the propulsive velocity decreases. Farooq *et al.* [18] studied the micropolar fluid within a uniform conduit with ciliated carpet on the inner walls where the results were verified by a comparison with those of Guha *et al.* [10]. Few relevant studies are given in the references [6–8, 20, 24].

With the above taken considerations, we wish to conduct theoretical research on the influence of electroosmotic pressures on traveling sperm through the flexible ciliated genital tract. To imitate the spermatic fluid with self-propulsive sperms, a hyperbolic tangent fluid is used as the base fluid. The perturbation method is mainly

used to solve the governing partial differential system of equations analytically. Because of the self-propulsion characteristic of swimmers and the approximation of long wavelength, a creeping stream routine is used throughout the canal. In addition to the pressure difference that is sought to affect the possibility of childbearing, the electroosmosis impact on the ciliated walls of the cervical channel is expected to have innovative implications. The current study provides a mathematical assessment of swimming sperms' interaction with electroosmosis through the ciliated vaginal canal where the embryo is affected by the interaction of ciliary activity, muscle contractions and tubal secretions [15]. This model investigates a number of factors, including propulsive velocity, streamlines of cervical flow, mucus velocities and pumping characteristics on the variables under consideration.

2. Electromagnetohydrodynamic propulsion for the non-Newtonian model

Consider a micro-organism (swimming sperms) moving inside a 2-D ciliated cervical conduit of a reproductive system of a female with speed V_p. Sperms are transported by self-propulsion in the shape of a flexible sheet that propels itself against the moving sinusoidal ripples on the canal walls that travel along the positive X-axis from the uterine tube to the vagina. Electroosmotic forces of a hyperbolic tangent fluid are sought to imitate the transient flow. The top swimming sheet is denoted by a plus sign, while the bottom one is denoted by a minus sign. The cartesian coordinates are employed in such a way that the X-axis is selected to run down the canal and the Y-axis is normal to it. The propagating oscillations along the walls of the cervical canal are assumed to have a speed c and a wavelength λ. We also suppose that the self-propelled flowing sheet of sperms moves in synchrony with the rotating frame of reference. The surface features of the cervical walls and the film of migrating sperms in the fixed frame, as shown in Figures 1 and 2, can be described as

Upper wall

$$h_1 = h_0 + b'_w \ \sin\left(\frac{2\pi}{\lambda}(X-(c-V'_p)t)\right) + 2\frac{Ab'_w}{\lambda}\pi\cos\left(\frac{2\pi k}{\lambda}(X-(c-V'_p)t)\right)\sin\left(\frac{2\pi}{\lambda}(X-(c-V'_p)t)\right)$$

Surface of swimming sperm $\quad h_s = b'_s \ \sin\left(\frac{2\pi}{\lambda}(X-(c-V'_p)t)+\phi\right)$

Lower wall

$$h_2 = -h_0 + b'_w \ \sin\left(\frac{2\pi}{\lambda}\left(X-\left(c-V'_p\right)t\right)\right) + 2\frac{Ab'_w}{\lambda}\pi\cos\left(\frac{2\pi k}{\lambda}(X-(c-V'_p)t)\right)\sin\left(\frac{2\pi}{\lambda}(X-(c-V'_p)t)\right) \tag{2.1}$$

where the mean distance travelled by the swimming sperm to another cervical membrane (lower or higher) is denoted by h_0, ϕ is the phase difference, and b'_s and b'_w are the wave amplitudes on the interface of the microorganism swimmer and the cervical surfaces, sequentially. In addition, Ab'_w are the material points at a maximal displacement, k is the constant and A is the amplitude of cilia's metachronal wave.

3. Cervical fluid equations

A motion of the incompressible cervical fluid is described by a hyperbolic tangent fluid and the motion of the governing equations is simulated in the 2D flow as follows

$$\rho\left(\frac{\partial \overrightarrow{q^{\pm}}}{\partial t} + \left(\overrightarrow{q^{\pm}}.\nabla\right)\overrightarrow{q^{\pm}}\right) = -\nabla p^{\pm} + \nabla.\tau^{\pm} + F, \tag{3.1}$$

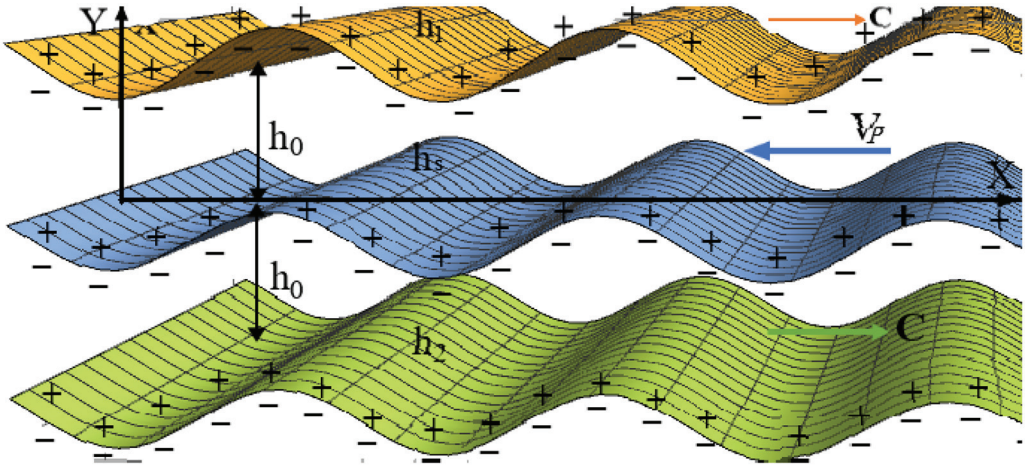

FIGURE 1. Diagram depicting the self-propulsion of a floating sheet of sperm cells *via* a female's cervical conduit.

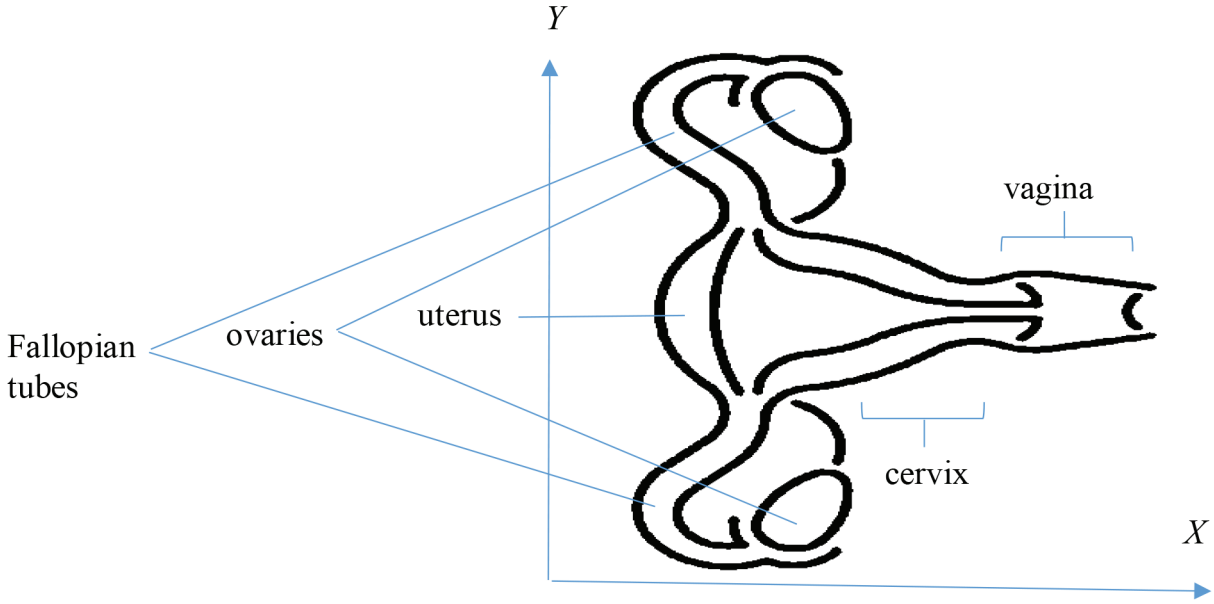

FIGURE 2. Anatomical diagram for the reproductive system of a female.

the stress tensor equation of the hyperbolic tangent fluid is defined as

$$\tau_{ij}{}^{\pm} = -\left\{\eta_\infty + (\eta_0 + \eta_\infty)\tanh\left(\Gamma\overline{\dot{\Lambda}}^{\pm}\right)^n\right\}\overline{\dot{\Lambda}}^{\pm}, \tag{3.2}$$

such that η_0 is the viscosity limiting shear rate and η_∞ is viscosity with infinite shear rate. Γ is a constant of time, n refers to the index of power law, and $\overline{\dot{\Lambda}}$ is defined as follows:

$$\overline{\dot{\Lambda}}^{\pm} = \sqrt{\frac{1}{2}\Pi^{\pm}} \tag{3.3}$$

where $\Pi^{\pm}$ is the second strain tensor invariant. By considering the infinite shear rate viscosity $\eta_\infty = 0$ and $\Gamma\overline{\dot{\Lambda}} \ll 1$, equation (3.2) can be written as:

$$\tau_{ij}{}^{\pm} = -\left\{\eta_0 + n\ \eta_0\left(\Gamma\overline{\dot{\Lambda}}^{\pm} - 1\right)\right\}\overline{\dot{\Lambda}}^{\pm} \tag{3.4}$$

We now analyze the EOF through the cervical canal. The density of the charge for the cervical fluid is given as follows:

$$\rho_e = \varepsilon\ e\ \left(n^+ - n^-\right) = -2\varepsilon\ e\ n_0\ \sinh\left\{\frac{\varepsilon\ e\overline{\varphi}}{k_B T_{av}}\right\}, \tag{3.5}$$

such that $n^- = n_0\ e^{\frac{\varepsilon\ e\overline{\varphi}}{k_B T_{av}}}$ and $n^+ = n_0\ e^{\frac{-\varepsilon\ e\overline{\varphi}}{k_B T_{av}}}$.

n^- *and* n^+ are the densities numbers of ions for both negative and positive, T_{av} is the absolute temperature, e is the electronic charge, ε is the ions' valence, k_B is Boltzmann constant, and n_0 is the bulk of volume concentration of negative or positive ions. In addition, using the linearization principle of Debye-Huckel $\left\{\frac{\varepsilon\ e\ \varphi'}{k_B T_{av}} \ll 1\right\}$, equation (3.5) reduces to

$$\rho_e{}^{\pm} = \frac{-\epsilon}{K^2}\ \overline{\varphi}^{\pm} \tag{3.6}$$

where $K = \sqrt{(\varepsilon\ e)^{-1}\frac{\epsilon\ k_B T_{av}}{2\ n_0}}$ is the Debye-Huckel parameter. Based on the Poisson-Boltzmann equation, the electroosmotic potential can be easily obtained as follows:

$$\frac{\partial^2\overline{\varphi}^{\pm}}{\partial\overline{x}^2} + \frac{\partial^2\overline{\varphi}^{\pm}}{\partial\overline{y}^2} = \frac{1}{K^2}\ \overline{\varphi}^{\pm}, \tag{3.7}$$

where ϵ is the dielectric constant and $\overline{\varphi}^{\pm}$ is the electroosmotic potential function.

The boundary conditions are given as

$$\begin{aligned} &\overline{w}^+ = 0, && \overline{\varphi}^+ = \zeta && at\ \overline{y} = h1(\overline{x}),\\ &\overline{w}^- = 0, && \overline{\varphi}^- = 0 && at\overline{y} = h2(\overline{x}),\\ &\overline{w}^{\pm} = 0, && \overline{\varphi}^{\pm} = \zeta && at\ \overline{y} = hs(\overline{x}), \end{aligned} \tag{3.8}$$

The equations governing the 2-D flow are then given by

$$\begin{aligned} &\frac{\partial U^{\pm}}{\partial X} + \frac{\partial V^{\pm}}{\partial Y} = 0,\\ &\rho\left(\frac{\partial U^{\pm}}{\partial t} + U^{\pm}\frac{\partial U^{\pm}}{\partial X} + V^{\pm}\frac{\partial U^{\pm}}{\partial Y}\right) = -\frac{\partial p^{\pm}}{\partial X} + \frac{\partial \tau_{XX}{}^{\pm}}{\partial X} + \frac{\partial \tau_{XY}{}^{\pm}}{\partial Y} + \rho_e{}^{\pm}E_X,\\ &\rho\left(\frac{\partial V^{\pm}}{\partial t} + U^{\pm}\frac{\partial V^{\pm}}{\partial X} + V^{\pm}\frac{\partial V^{\pm}}{\partial Y}\right) = -\frac{\partial p^{\pm}}{\partial Y} + \frac{\partial \tau_{YX}{}^{\pm}}{\partial X} + \frac{\partial \tau_{YY}{}^{\pm}}{\partial Y}, \end{aligned} \tag{3.9}$$

The relation of the fixed and moving (laboratory) reference frames are as follows

$$\begin{aligned} \tilde{x} &= X - \left(c - V_p'\right) t, \qquad \tilde{y} = Y, \\ \tilde{u}^{\pm} &= U^{\pm} - \left(c - V_p'\right), \quad \tilde{v}^{\pm} = V^{\pm}. \end{aligned} \tag{3.10}$$

Considering equation (3.10), the governing equation (3.9) of the cervical fluid become

$$\begin{aligned} \frac{\partial \tilde{u}^{\pm}}{\partial x} + \frac{\partial \tilde{v}^{\pm}}{\partial y} &= 0, \\ \rho \left(\tilde{u}^{\pm} \frac{\partial \tilde{u}^{\pm}}{\partial \tilde{x}} + \tilde{v}^{\pm} \frac{\partial \tilde{u}^{\pm}}{\partial \tilde{y}} \right) &= -\frac{\partial \tilde{p}^{\pm}}{\partial \tilde{x}} + \frac{\partial {\tau_{\tilde{x}\tilde{x}}}^{\pm}}{\partial \tilde{x}} + \frac{\partial {\tau_{\tilde{x}\tilde{y}}}^{\pm}}{\partial \tilde{y}} + {\rho_e}^{\pm} E_{\tilde{x}}, \\ \rho \left(\tilde{u}^{\pm} \frac{\partial \tilde{v}^{\pm}}{\partial \tilde{x}} + \tilde{v}^{\pm} \frac{\partial \tilde{v}^{\pm}}{\partial \tilde{y}} \right) &= -\frac{\partial \tilde{p}^{\pm}}{\partial \tilde{y}} + \frac{\partial {\tau_{\tilde{y}\tilde{x}}}^{\pm}}{\partial \tilde{x}} + \frac{\partial {\tau_{\tilde{y}\tilde{y}}}^{\pm}}{\partial \tilde{y}}, \end{aligned} \tag{3.11}$$

We introduce the following dimensionless parameters:

$$\begin{aligned} \tilde{x} = \frac{x}{\lambda}, \tilde{y} = \frac{y}{h_0}, \ \tilde{u}^{\pm} = \frac{u^{\pm}}{c}, \ \tilde{v}^{\pm} = \frac{v^{\pm}}{\delta c}, \\ \tilde{p}^{\pm} = \frac{h_0^2}{\lambda \mu c^2}, \ \delta = \ \frac{h_0}{\lambda}, \ b_s = \frac{{b'}_s}{h_0} \ , \ b_w = \frac{{b'}_w}{h_0}, \text{and} V_p' = \frac{V_p}{c}. \end{aligned} \tag{3.12}$$

By making use of the non-dimensional parameters given in equation (3.12) and the Eyring- Powell definition of fluid in equation (3.4), the non-dimensional equations for the model can be given by

$$\begin{aligned} R_e \ \delta \left(u^{\pm} \frac{\partial u^{\pm}}{\partial x} + v^{\pm} \frac{\partial u^{\pm}}{\partial y} \right) &= -\frac{\partial p^{\pm}}{\partial x} + \delta^2 \frac{\partial {\tau_{xx}}^{\pm}}{\partial x} + \frac{\partial {\tau_{xy}}^{\pm}}{\partial y} + m^2 U_{HS} \varphi^{\pm}, \\ R_e \ \delta^3 \left(u^{\pm} \frac{\partial v^{\pm}}{\partial x} + v^{\pm} \frac{\partial v^{\pm}}{\partial y} \right) &= -\frac{\partial p^{\pm}}{\partial y} + \delta^2 \frac{\partial {\tau_{xy}}^{\pm}}{\partial x} + \delta \frac{\partial {\tau_{yy}}^{\pm}}{\partial y}, \end{aligned} \tag{3.13}$$

where $R_e \ (= \frac{\rho c h_0}{\mu})$ is Reynolds number. Using the approximation $\delta = \ \frac{2\pi h_0}{\lambda} \ll 1$. Then, equation (3.13) becomes

$$\begin{aligned} 0 = -\frac{\partial p^{\pm}}{\partial x} + (1-n) \frac{\partial^2 u^{\pm}}{\partial y^2} + n \ W_e \ \frac{\partial}{\partial y} \left(\frac{\partial^2 u^{\pm}}{\partial y^2} \right)^2 + m^2 U_{HS} \varphi^{\pm}(y), \\ 0 = -\frac{\partial p^{\pm}}{\partial y}, \end{aligned} \tag{3.14}$$

and the associated boundary conditions

$$\begin{aligned} u^{\pm} &= V_p - 1 \ at \ y = \ h_{1,2}, \\ u^{\pm} &= -1 \ at \ y = h_s. \end{aligned} \tag{3.15}$$

where $h_1 = 1 + b_w \ \sin(2\pi x) \ + b_w \varphi \cos(2\pi k x) \sin(2\pi x)$, $h_2 = -1 + b_w \ \sin(2\pi x) \ + b_w \varphi \cos(2\pi k x) \sin(2\pi x)$ and $h_s = b_s \ \sin(2\pi \ (x + \varphi))$, where φ denotes the metachronal wave parameter.

4. Methodology solution

Because equation (3.14) is a nonlinear PDE, a closed form solution is not attainable. Furthermore, it may be solved analytically using the perturbation technique in terms of the small parameter We (Weissenberg number)

by extending $p^{\pm}$ and $F^{\pm}$ in the following ways:

$$\begin{aligned} u^{\pm}(y) &= {u_0}^{\pm}(y) + W_e\ {u_1}^{\pm}(y) + O\left({W_e}^2\right), \\ p^{\pm}(y) &= {p_0}^{\pm}(y) + W_e\ {p_1}^{\pm}(y) + O\left({W_e}^2\right), \\ F^{\pm}(y) &= {F_0}^{\pm}(y) + W_e\ {F_1}^{\pm}(y) + O({W_e}^2). \end{aligned} \tag{4.1}$$

Plugging the above expressions in equation (3.14) and the boundary conditions equation (3.15), we get thefollowing systems:

4.1. Zero order equations of (W_e^0)

$$0 = -\frac{\partial {p_0}^{\pm}}{\partial x} + (1-n)\frac{\partial^2 {u_0}^{\pm}}{\partial y^2} + m^2 U_{HS}\varphi^{\pm}(y), \tag{4.2}$$

with associated boundary conditions

$$\begin{aligned} {u_0}^{\pm} &= V_p - 1\ at\ y = \ h_{1,2}, \\ {u_0}^{\pm} &= -1\ at\ y = h_s. \end{aligned} \tag{4.3}$$

4.2. First order equations of (W_e)

$$0 = -\frac{\partial {p_1}^{\pm}}{\partial x} + (1-n)\frac{\partial^2 {u_1}^{\pm}}{\partial y^2} + 2n\ \frac{\partial u_0}{\partial y}\frac{\partial^2 {u_0}^{\pm}}{\partial y^2} \tag{4.4}$$

with associated boundary conditions

$$\begin{aligned} {u_1}^{\pm} &= 0\ at\ y = \ h_{1,2}, \\ {u_1}^{\pm} &= 0\ at\ y = h_s. \end{aligned} \tag{4.5}$$

Zero order solutions

Using the boundary conditions (4.3), the solution of equation (4.2) of the upper and lower flow takes the form:

Cervical Upper Fluid

$$\begin{aligned} u^{+}(y) = &\frac{\partial {p_0}^{+}}{\partial x}\frac{(h_1-y)(-h_s+\mathrm{y})}{2(-1+n)} + \frac{1}{2(h_2-h_s)(-1+n)}\Bigg(2\ h_1 - 2\ h_s - 2n\ h_1 - 2n\ h_s\,(-1+V_p) \\ &+2h_sV_p - 2h_sU_{HS} + 2y\left((-1+n)\,V_p + U_{HS}\right) + 2U_{HS}(h_1-h_s)\frac{\sinh\left(m(h_s-y)\right)}{\cosh\left(m(h_1-h_s)\right)}\Bigg), \end{aligned} \tag{4.6}$$

Cervical Lower Fluid

$$\begin{aligned} u^{-}(y) = &\frac{\partial p^{-}}{\partial x}\frac{(h_2-y)(-h_s+\mathrm{y})}{2(-1+n)} + \frac{1}{2(h_2-h_s)(-1+n)}\Bigg(2\ h_2 - 2\ h_s - 2n\ h_2 - 2n\ h_s\,(-1+V_p) \\ &+2h_sV_p - 2h_sU_{HS} + 2y\left((-1+n)\,V_p + U_{HS}\right) + 2U_{HS}(h_2-h_s)\frac{\sinh\left(m(h_s-y)\right)}{\cosh\left(m(h_2-h_s)\right)}\Bigg), \end{aligned} \tag{4.7}$$

First order solutions Using the boundary conditions (4.5) and using the zero order solutions (4.6) and (4.7), the solution of equation (4.4) of the upper and lower flow takes the form:

Cervical Upper Fluid

$$
\begin{aligned}
u_i^{\pm}(y) = {} & \frac{\partial p_i^{\pm}}{\partial x}\frac{(h_i-y)(-h_s+y)}{2(-1+n)} + \frac{m_e\ n\ Csch[(h_i-\ h_s)\ m_e]^2}{12(h_i-\ h_s)^2\ m_e(-1+n)^3}\Bigg(\Big(\ h_s-y\Big)\Bigg(-(h_i-\ h_s)\ \frac{\partial p_0^{\pm}}{\partial x}\Bigg(6(-1 \\
& +n)V_P + (h_i-\ h_s)\frac{\partial p_0^{\pm}}{\partial x}(h_i+\ h_s-2y)\Bigg)\Big(\ h_1-y\Big) - 6\Bigg(2(-1+n)V_P + \Big(\ h_i-\ h_s\Big)\frac{\partial p_0^{\pm}}{\partial x}\Big(\ h_s \\
& -y\Big)\Bigg)U_{HS} - 12{U_{HS}}^2\Bigg) - \ m_e\Big(\ h_s-y\Big)\Bigg(-(h_i-\ h_s)\frac{\partial p_0^{\pm}}{\partial x}\Bigg(6(-1+n)V_P + (h_i \\
& -\ h_s)\frac{\partial p_0^{\pm}}{\partial x}(h_i+\ h_s-2y)\Big)(h_i-y) - 6\Bigg(2(-1+n)V_P + (h_i-\ h_s)\frac{\partial p_0^{+}}{\partial x}\Big(\ h_s-y\Big)\Big)U_{HS} \\
& -12{U_{HS}}^2\Bigg)\cosh[2(h_i-\ h_s)\ m_e] + 3(h_i-\ h_s)U_{HS}\ \Bigg(-2\ m_e\Bigg(\Big(\ h_i-\ h_s\Big)\frac{\partial p_0^{\pm}}{\partial x}\Big(\ h_i+\ h_s-2y\Big) \\
& +2((-1+n)V_P+\beta)\Bigg)\cosh[\ m_e\Big(\ h_i-y\Big)] + 2\ m_e\Bigg(\Big(\ h_i-\ h_s\Big)\frac{\partial p_0^{+}}{\partial x}\Big(\ h_i+\ h_s-2y\Big) \\
& +2((-1+n)V_P+U_{HS})\Bigg)\cosh[\ m_e(h_i-2\ h_s+y)] - 8\ h_i\frac{\partial p_0^{+}}{\partial x}\ \sinh[(h_i-\ h_s)\ m_e] \\
& +8\ \frac{\partial p_0^{+}}{\partial x}\ y\ \sinh[(h_i-\ h_s)\ m_e] + 4\ h_s\frac{\partial p_0^{+}}{\partial x}\sinh[2(h_i-\ h_s)\ m_e] - 4\ \frac{\partial p_0^{+}}{\partial x}\ y\ \sinh[2(h_i \\
& -\ h_s)\ m_e] - \ h_s\ \ {m_e}^2U_{HS}\ \sinh[2(\ h_i-\ h_s)\ m_e] + \ {m_e}^2\ y\ U_{HS}\ \sinh[2(h_i-\ h_s)\ m_e] \\
& +4h_i\frac{\partial p_0^{+}}{\partial x}\ \sinh[\ m_e(h_i-y)] - 4\ h_s\ \frac{\partial p_0^{+}}{\partial x}\ \sinh[\ m_e(h_i-y)] + h_i\ {m_e}^2U_{HS}\ \sinh[2\ m_e\Big(\ h_s \\
& -y\Big)] - \ h_s\ {m_e}^2U_{HS}\ \sinh[2\ m_e\Big(\ h_s-y\Big)] + 4(h_i-\ h_s)\ \frac{\partial p_0^{+}}{\partial x}\ \sinh[\ m_e(h_i-2\ h_s+y)]\Big)\Bigg).
\end{aligned}
\tag{4.8}
$$

5. Swimming sheet propulsive velocity

Integrating the continuity equation reveals that the flow rates of self-propelled sperm cells above and below the floating sheet remain constant. Furthermore, because the pressure differential throughout the wavelength, Δp, is constant in both zones, the volumetric flow rate throughout the channel Q may be calculated using the formula

$$
Q^- = \int_{h_2}^{h_s} u^-(y)\ \mathrm{d}y,\ Q^+ = \int_{h_s}^{h_1} u^+(y)\ \mathrm{d}y, \tag{5.1}
$$

Using equations (4.7)–(4.8), equation (4.8) takes the forms

$$
\begin{aligned}
\Delta p &= I_1 + I_2\ Q^+ + I_3\ V_P, \\
\Delta p &= I_4 + I_5\ Q^- + I_6\ V_P,
\end{aligned}
\tag{5.2}
$$

where

$$I_1 = \int_0^1 \frac{12(-1+n)}{(\ h_{\mathbf{1}} - h_{\mathbf{3}})^3} \mathrm{d}x,$$

$$I_2 = \int_0^1 F1\Bigg(-2(\ h_{\mathbf{1}} - h_{\boldsymbol{s}})\ m_e \Bigg(-3\ h_{\mathbf{1}}(-1+n)^2 + \ h_{\mathbf{1}}{}^2 n \frac{\partial p_0{}^+}{\partial x}\ W_e + \ h_{\mathbf{1}}{}^2 n \frac{\partial p_0{}^+}{\partial x}\ W_e$$
$$+ h_{\mathbf{1}} \Bigg(3 + 3n^2 - 2n \Big(3 + \ h_{\mathbf{1}} \frac{\partial p_0{}^+}{\partial x}\ W_e \Big) \Bigg) + 6n\ W_e\ U_{HS} \Bigg)$$
$$+24n\ W_e\ U_{HS}\ \mathrm{Tanh}[\frac{1}{2}(\ h_{\mathbf{1}} - h_{\boldsymbol{s}})\ m_e] \Bigg) \mathrm{d}x,$$

$$I_3 = \int_0^1 F_1 \Bigg((\ h_{\mathbf{1}} - h_{\mathbf{3}})(12(\ h_{\mathbf{1}} - h_s)\ m_e{}^2(-1+n)^3 - 6(\ h_{\mathbf{1}} - h_{\boldsymbol{s}})\ m_e{}^2(-1+n)^2 U_{HS}$$
$$+4(12 + (\ h_{\mathbf{1}} - h_{\boldsymbol{s}})^2\ m_e{}^2) n \frac{\partial p_0{}^+}{\partial x}\ W_e\ U_{HS} - 15\ m_e{}^2 n\ W_e U_{HS}{}^2)$$
$$+3\ m_e U_{HS}((4(\ h_{\mathbf{1}} - h_{\boldsymbol{s}})((-1+n)^2 + 2(\ -h_{\mathbf{1}} + h_{\boldsymbol{s}}) n \frac{\partial p_0{}^+}{\partial x}\ W_e) + (8$$
$$+(\ h_{\mathbf{1}} - h_{\boldsymbol{s}})^2\ m_e{}^2) n\ W_e U_{HS})\mathrm{Coth}[(\ h_{\mathbf{1}} - h_{\boldsymbol{s}})\ m_e] - 4((\ h_{\mathbf{1}} - h_{\boldsymbol{s}})((-1+n)^2$$
$$+2(\ h_{\mathbf{1}} - h_{\boldsymbol{s}}) n \frac{\partial p_0{}^+}{\partial x}\ W_e) + 2n\ W_e\ U_{HS})\mathrm{Csch}[(\ h_{\mathbf{1}} - h_{\boldsymbol{s}})\ m_e]) \Bigg) \mathrm{d}x,$$

$$I_4 = \int_0^1 \frac{12(-1+n)}{(\ h_{\mathbf{2}} - \ h_{\boldsymbol{s}})^3} \mathrm{d}x,$$

$$I_5 = \int_0^1 F2 \Bigg(-2(\ h_{\mathbf{2}} - \ h_{\boldsymbol{s}})\ m_e \Bigg(-3\ h_{\boldsymbol{s}}(-1+n)^2 + \ h_{\mathbf{2}}{}^2 n \frac{\partial p_0{}^-}{\partial x}\ W_e$$
$$+ h_{\boldsymbol{s}}{}^2 n \frac{\partial p_0{}^-}{\partial x}\ W_e + \ h_{\mathbf{2}} \Bigg(3 + 3n^2 - 2n \Big(3 + \ h_{\boldsymbol{s}} \frac{\partial p_0{}^-}{\partial x}\ W_e \Big) \Bigg) + 6n\ W_e U_{HS} \Bigg)$$
$$+24n\ W_e\ U_{HS}\ \mathrm{Tanh}\left[\frac{1}{2}(\ h_{\mathbf{2}} - \ h_{\boldsymbol{s}})\ m_e \right] \Bigg) \mathrm{d}x,$$

$$I_6 = \int_0^1 F_2 \Bigg((\ h_{\mathbf{2}} - \ h_{\boldsymbol{s}}) \Big(12(\ h_{\mathbf{2}} - \ h_{\boldsymbol{s}})\ m_e{}^2(-1+n)^3 - 6(\ h_{\mathbf{2}} - \ h_{\boldsymbol{s}})\ m_e{}^2(-1+n)^2 U_{HS}$$
$$+4(12 + (\ h_{\mathbf{2}} - \ h_{\boldsymbol{s}})^2\ m_e{}^2) n \frac{\partial p_0{}^-}{\partial x}\ W_e U_{HS} - 15\ m_e{}^2 n\ W_e U_{HS}{}^2 \Big)$$
$$+3\ m_e\ U_{HS} \Bigg(\Big(4(\ h_{\mathbf{2}} - \ h_{\boldsymbol{s}}) \Big((-1+n)^2 + 2(-h_{\mathbf{2}} + \ h_{\boldsymbol{s}}) n \frac{\partial p_0{}^-}{\partial x}\ W_e \Big)$$
$$+(8 + (\ h_{\mathbf{2}} - \ h_{\boldsymbol{s}})^2\ m_e{}^2) n\ W_e\ U_{HS} \Big) \mathrm{Coth}[(\ h_{\mathbf{2}} - \ h_{\boldsymbol{s}})\ m_e]$$
$$-4 \Bigg((\ h_{\mathbf{2}} - \ h_{\boldsymbol{s}}) \Big((-1+n)^2 + 2(\ h_{\mathbf{2}} - \ h_{\boldsymbol{s}}) n \frac{\partial p_0{}^-}{\partial x}\ W_e \Big)$$

$$+2n\ W_e\ U_{HS})\mathrm{Csch}[(\ h_{\boldsymbol{2}} -\ h_{\boldsymbol{s}}\Big)\ m_e]\Big)\Big)\mathrm{d}x,$$

and

$$F_i = \frac{1}{(\ h_{\boldsymbol{i}} -\ h_{\boldsymbol{3}})^4 m(-1+n)}.$$

Because the moving sheet of sperm cells is self-propulsive, the forces imposed by the fluid on it must balance in order for its motion to remain of constant velocity V_P [21]. This may be mathematically expressed as

$$\int_0^1 \left({\tau_{xy}}^+ - {\tau_{xy}}^- - b_s \sin 2\pi x\ \left(\frac{\partial p^+}{\partial x} - \frac{\partial p^-}{\partial x}\right)\right) \mathrm{d}x = 0, \tag{5.3}$$

Using Mathematica Software Program to solve equations (5.2), (5.3) and find the self-propulsive spermatozoa velocity V_P.

The energy dissipated by the micro-swimmer is given as

$$\int_{-1}^1 b_s \cos 2\pi x\ \left(\frac{\partial p^+}{\partial x} - \frac{\partial p^-}{\partial x}\right) \mathrm{d}x \tag{5.4}$$

6. Results and discussion

The purpose of this section is to study the influence of relevant factors on the expressions corresponding with the flow regime. Mathematica is used to express the actual effect of the non-Newtonian fluid parameter $\boldsymbol{W_e}$ (Weissenberg number), electroosmotic parameter $\boldsymbol{m_e}$, Helmholtz-Smoluchowski velocity $\boldsymbol{U_{HS}}$, metachronal parameter $\boldsymbol{\varphi}$, velocity of swimming sheet $\boldsymbol{V_p}$ on the behaviour of pressure difference over wavelength $\boldsymbol{\Delta p}$, streamlines and mucus velocities of cervical conduit $\boldsymbol{u^{\pm}}$. Because the topic encompasses lower and upper traveling layers, the negative and positive superscripts for each outcome variable under investigation signify the lower and upper swimming layers, respectfully, in the ongoing discussion.

6.1. Streamlines of cervical flow

Figures 3–10 are plotted to examine the impacts of the relevant parameters on the streamlines modality of the lubricious cervical conduit. Figures 3 and 4 are made to study the effect of non-Newtonian parameter W_e on the behaviour of the streamlines of cervical flow. It is seen that the trapped zones increase by increasing W_e in the lower and upper swimming sheets. Figures 5 and 6 simulate the streamlines behaviour for diverse values n where it is seen that the number of trapped bolus is enhanced through the region of the upper sheet but decreased in the lower region. Also, it is elucidated that in the same figures that the trapped bolus size is reduced for both sheets. Figures 7 and 8 display the behaviour of streamlines for different values of Helmholtz-Smoluchowski velocity U_{HS}. It is depicted that the increase in U_{HS} implies to a decrease in the size and number of trapped bolus through both sheets (upper and lower). Figures 9 and 10 elucidate the effect of electroosmotic parameter on the behaviour of streamlines. It is seen that as the electroosmotic parameter increases the size and number of bolus decreases through the upper sperm sheet but increases through the lower region of swimming sheet.

6.2. Mucus velocities

Figures 11a–f simulates the mucus velocities demeanour for many values of the parameters associated with the study. The mucus velocities are plotted versus y for the upper and lower swimming sheets of spermatozoa. Figure 11a discusses the effect W_e where it is demonstrated that as W_e increases, the demeanour of mucus velocity profile decreases below the swimming sheet whereas the behavior is completely overturned around

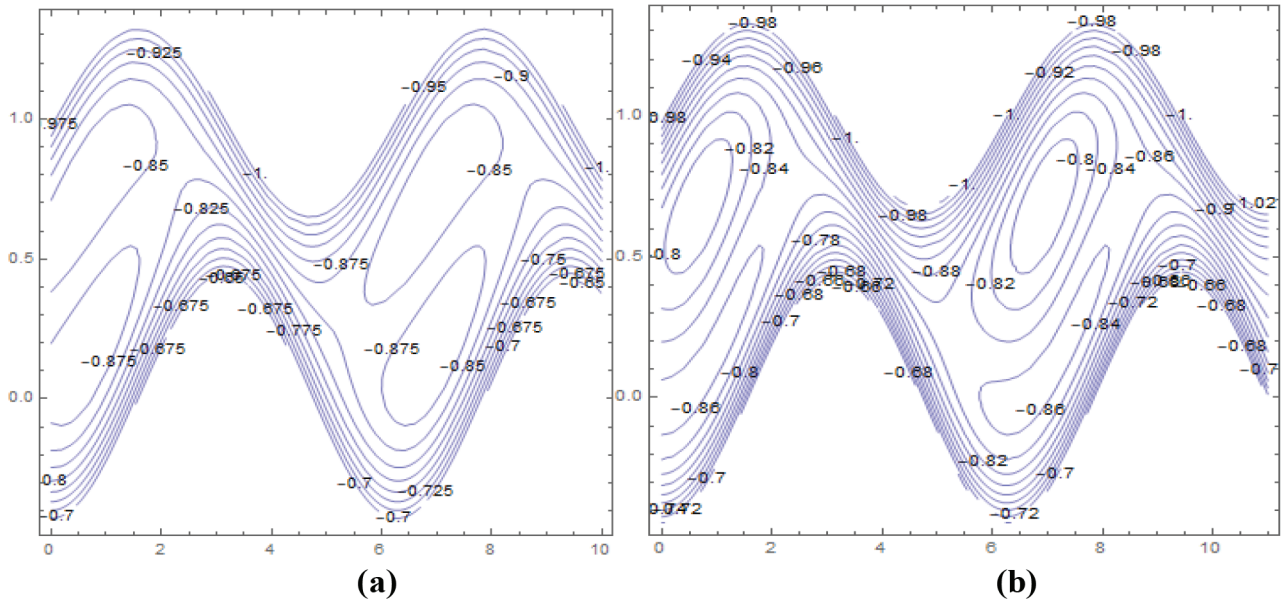

FIGURE 3. Streamlines of flow above the swimming sheet for $W_e = 0$ (panel a), $W_e = 0.5$ (panel b) with $V_p = 0.1$, $b_w = 0.35$, $b_s = 0.45$, $Q = -0.323$, $\phi = \pi/2$.

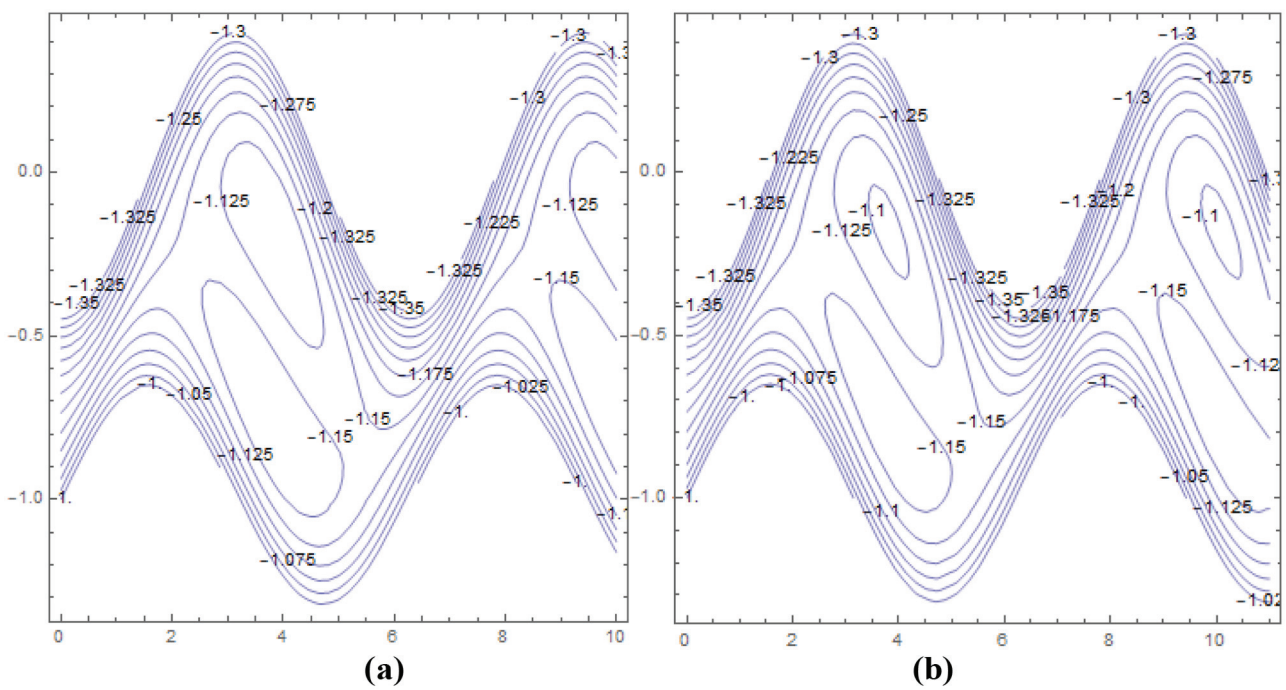

FIGURE 4. Streamlines of flow below the swimming sheet for $W_e = 0$ (panel a), $W_e = 0.5$ (panel b) with $V_p = 0.1$, $b_w = 0.35$, $b_s = 0.45$, $Q = -0.323$, $\phi = \pi/2$.

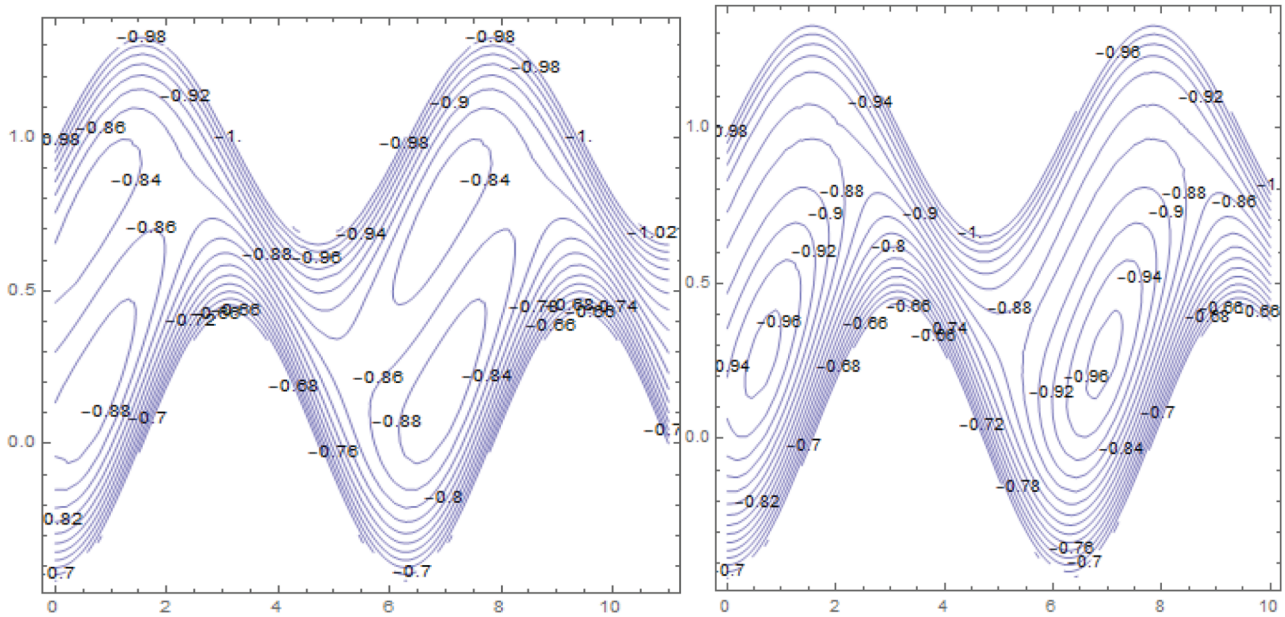

(a) **(b)**

FIGURE 5. Streamlines of flow upper the swimming sheet for $n = 2$ (panel a), $n = 2.1$ with $b_w = 0.35$, $b_s = 0.45$, $Q = -0.323$, $\phi = \pi/2$.

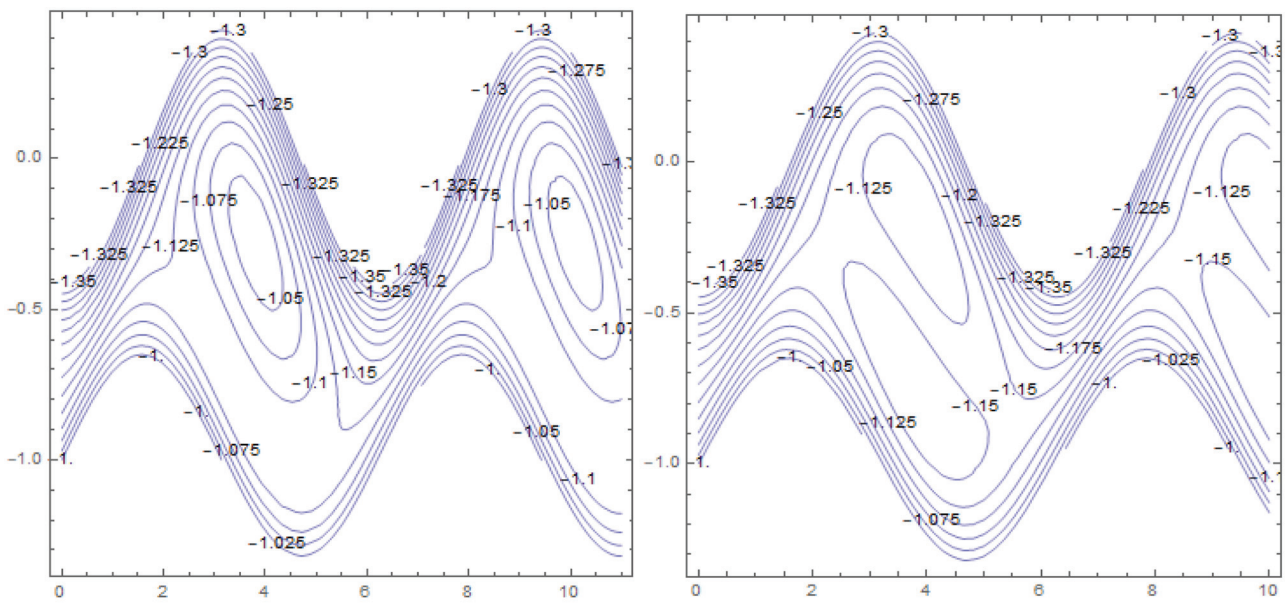

(a) **(b)**

FIGURE 6. Streamlines of flow lower the swimming sheet for $n = 2$ (panel a), $n = 2.1$ with $b_w = 0.35$, $b_s = 0.45$, $Q = -0.323$, $\phi = \pi/2$.

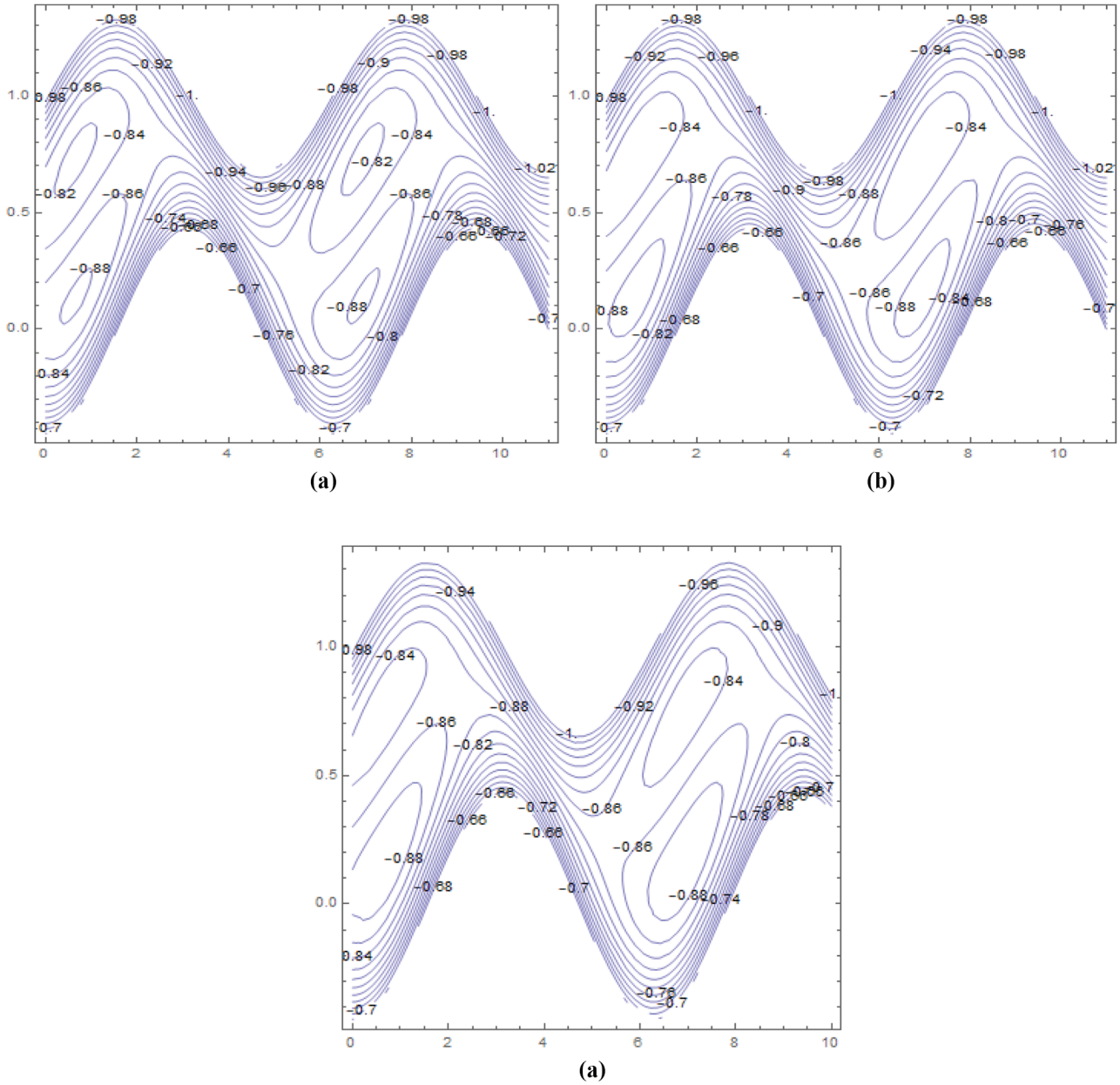

FIGURE 7. Streamlines of flow above the swimming sheet for $U_{HS} = -1$ (panel a) and $U_{HS} = 0$ (panel b), $U_{HS} = 1$ (panel c) with $b_w = 0.35$, $b_s = 0.45$, $Q = -0.323$, $\phi = \pi/2$, $V_p = 0.1$.

down the region of the swimming sheet. This effect shows that the rheological effect of hyperbolic tangent fluid is more appropriate to simulate and discuss the motility of cervical fluid. Figures 11b, c depicts the various values of the m_e and U_{HS} on the behaviour of $u^{\pm}$ *versus* y. It is demonstrated that the flow accelerates in both regions (lower and upper regions of floating sheet) with an increase in m_e and U_{HS}. It is also demonstrated that the mucus velocity slightly increases through the lower region of swimming sheet. Figure 11d exhibits the impact of different values of n on the mucus velocities. It is seen that as n increases, the mucus velocity decreases at the

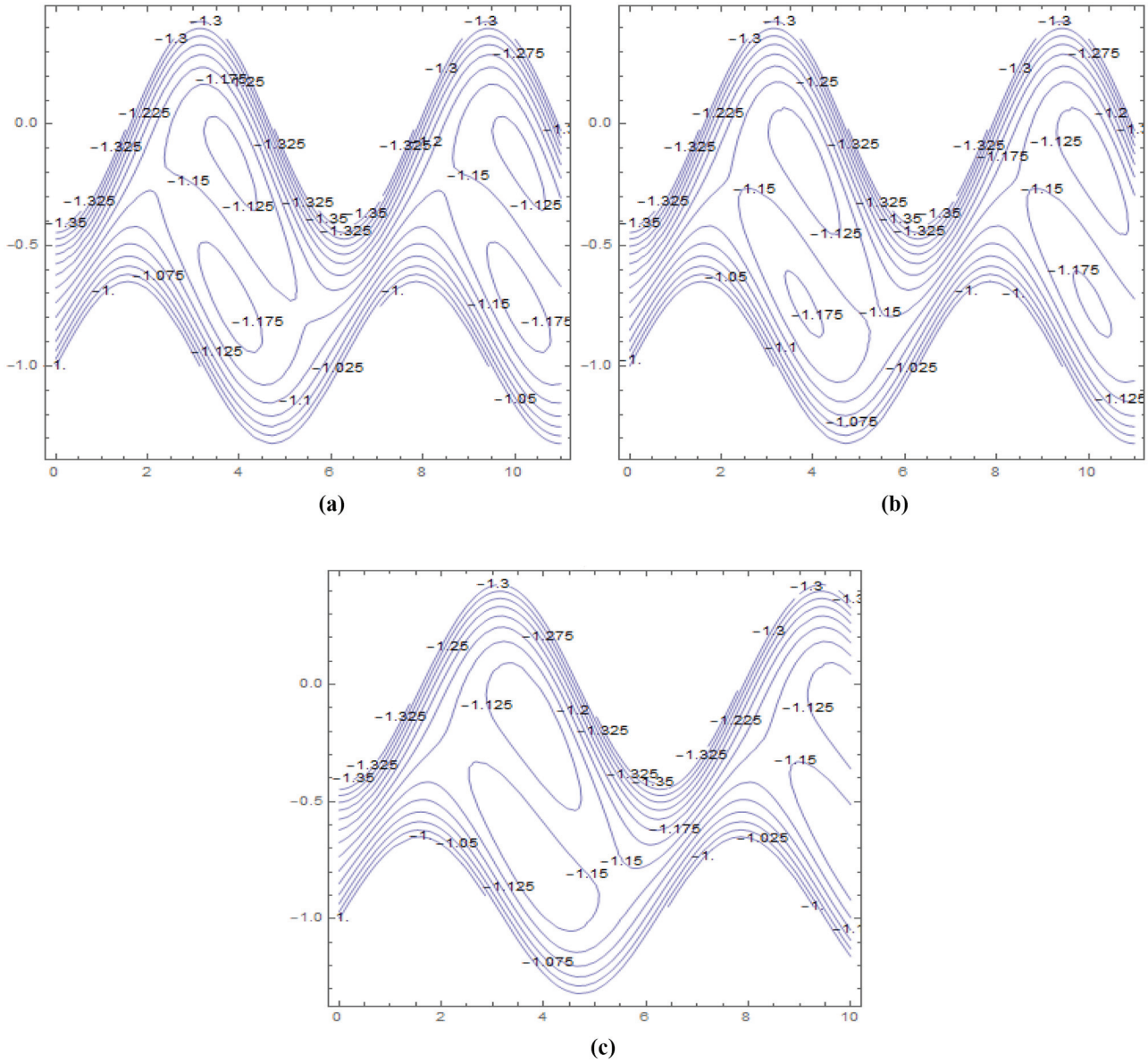

FIGURE 8. Streamlines of flow lower the swimming sheet for $U_{HS} = -1$ (panel a) and $U_{HS} = 0$ (panel b), $U_{HS} = 1$ (panel c) with $b_w = 0.35$, $b_s = 0.45$, $Q = -0.323$, $\phi = \pi/2$, $V_p = 0.1$.

region above the swimming sheet, whereas an opposite effect appears at the region down the swimming sheet. This effect refers to the motility of mucus velocity being more applicable for small values of n at the above swimming sheet of propulsive spermatozoa velocity. Figure 11e shows the impact of the metachronal parameter on the mucus velocity. It was observed when the metachronal parameter increases the mucus velocity increases above and below the swimming sheet. In addition, from Figure 11e, the peristaltic ciliary flow and the peristaltic flow are compared. It can be seen that the mucus velocity has the least values in the case of peristaltic flow field, and it is increases continuously in the case of peristaltic ciliary flow. Figure 11f reveals the motility of

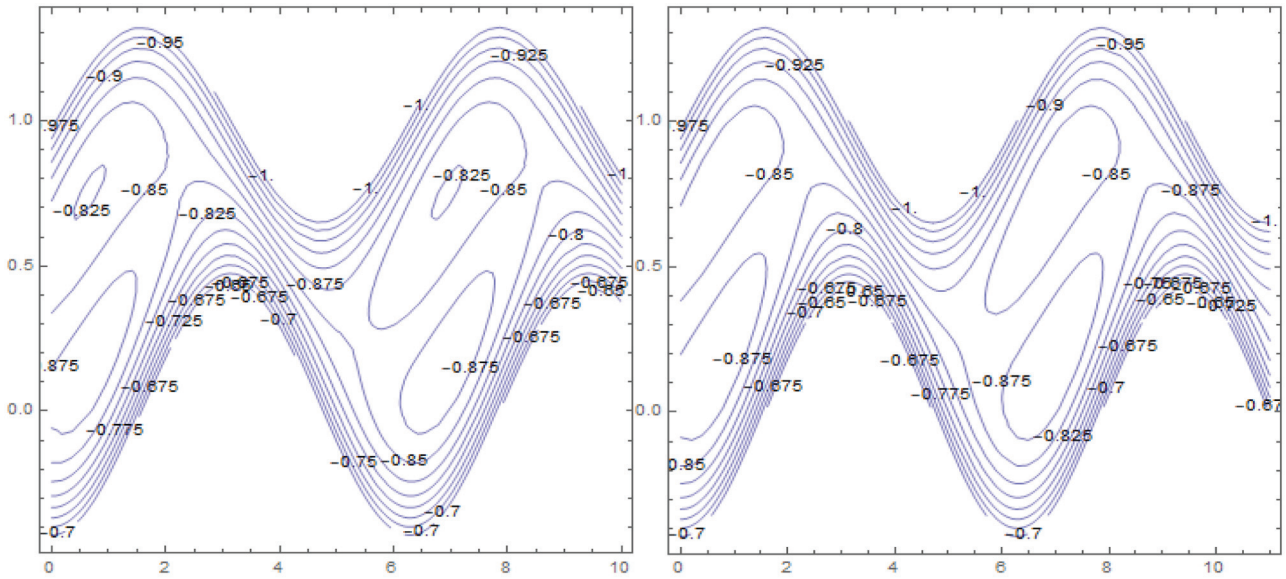

(a) **(b)**

FIGURE 9. Streamlines of flow upper the swimming sheet for $m = 1$ (panel a), $m = 2$ (panel b) with $b_w = 0.35$, $b_s = 0.45$, $Q = -0.323$, $\phi = \pi/2$.

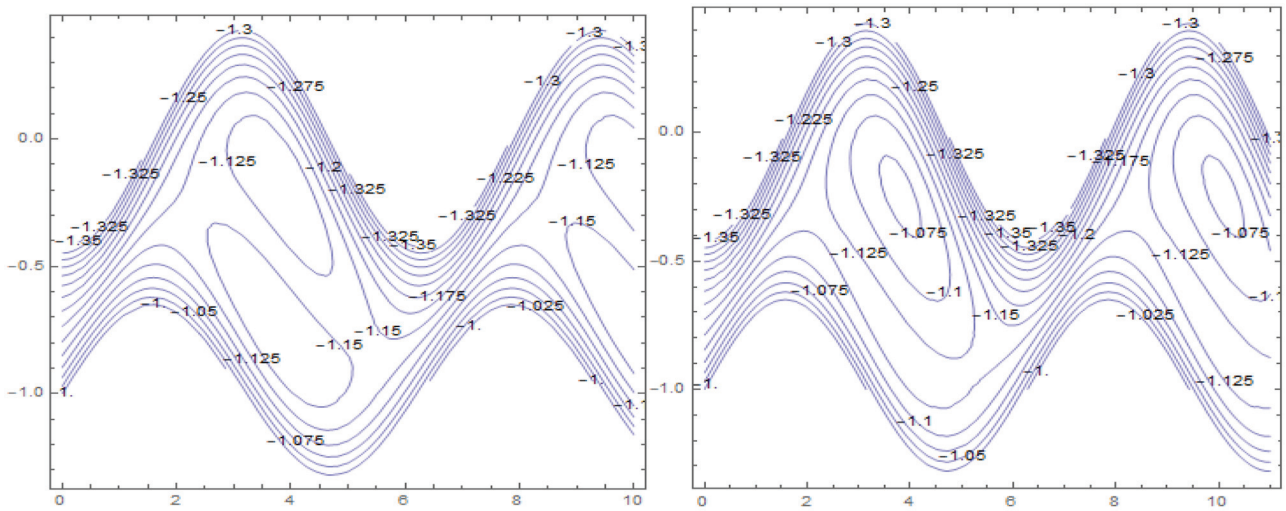

(a) **(b)**

FIGURE 10. Streamlines of flow below the swimming sheet for $m = 1$ (panel a), $m = 2$ (panel b) with $b_w = 0.35$, $b_s = 0.45$, $Q = -0.323$, $\phi = \pi/2$.

mucus velocity for sundry values of the propulsive velocity of swimming sheet V_p. It is revealed that the mucus velocity is enhanced substantially through both regions of the swimming sheet.

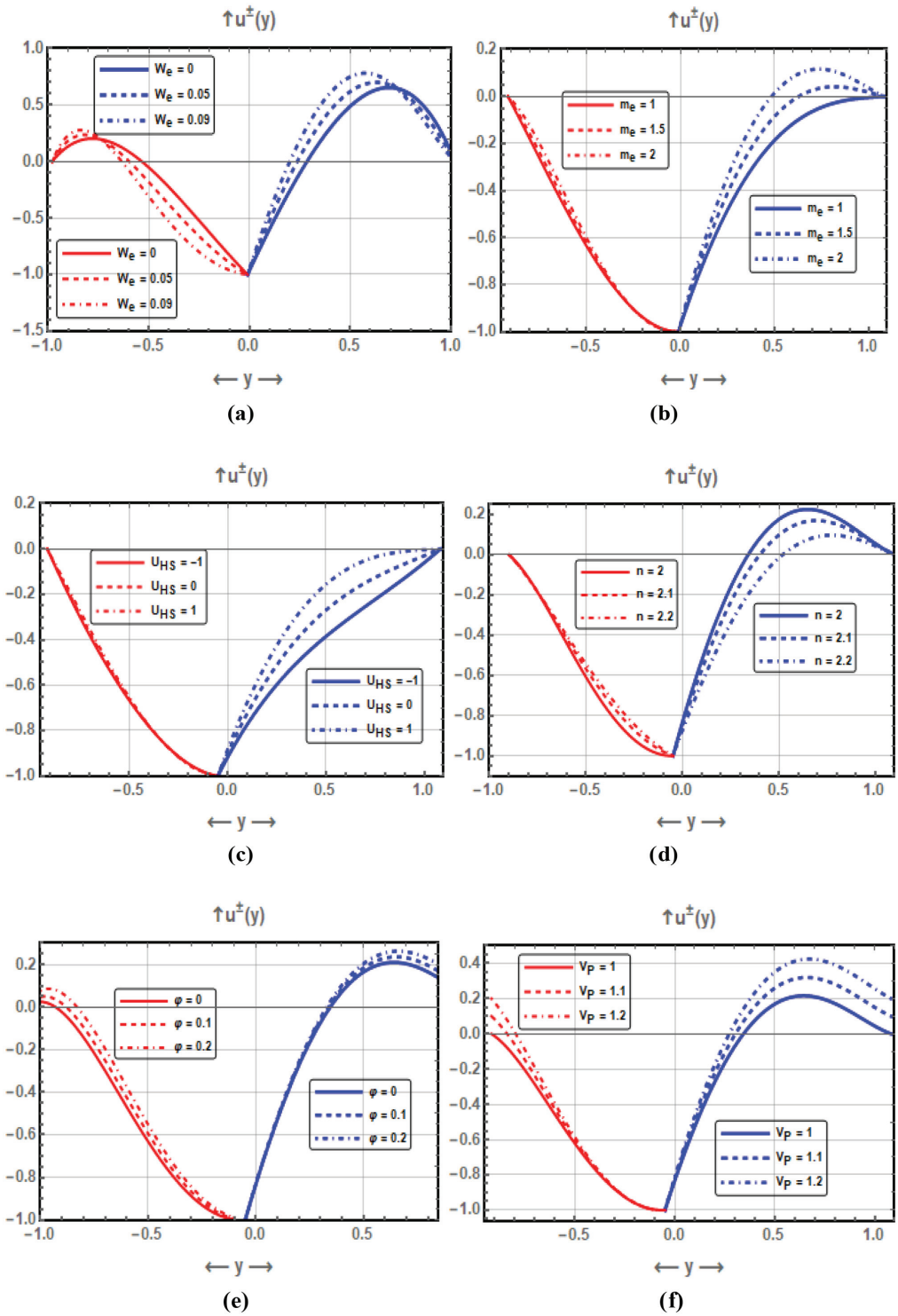

FIGURE 11. Plots for mucus velocities below and above the swimming sheet: for various values of α with $V_p = 0.1$, $b_w = 0.1$, $b_s = 0.01$, $\phi = \pi/2$, $Q = -0.1$, and $x = 0.2$ (panel a); W_e with (panel b); 2 (panel c).

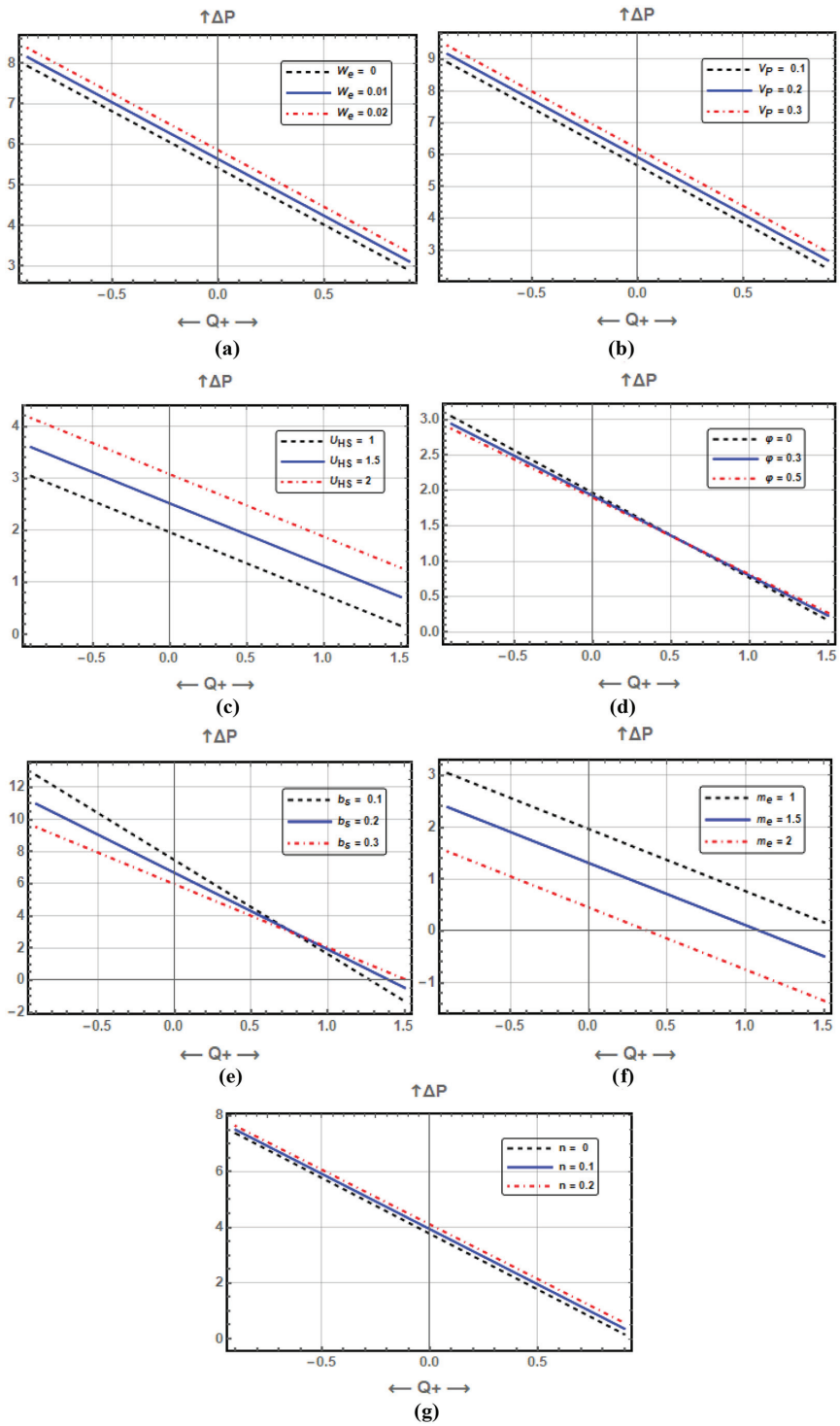

FIGURE 12. Plots for pressure rise versus mean flow rate at $b_w = 0.1$, $\phi = \pi$, $\alpha = 0.1$, $b_s = 0.1$: for various values of W_e (Panel a), V_p (Panel b), U_{HS} (Panel c), φ (Panel d), b_s (Panel e), m_e (Panel f) ,and n (Panel g).

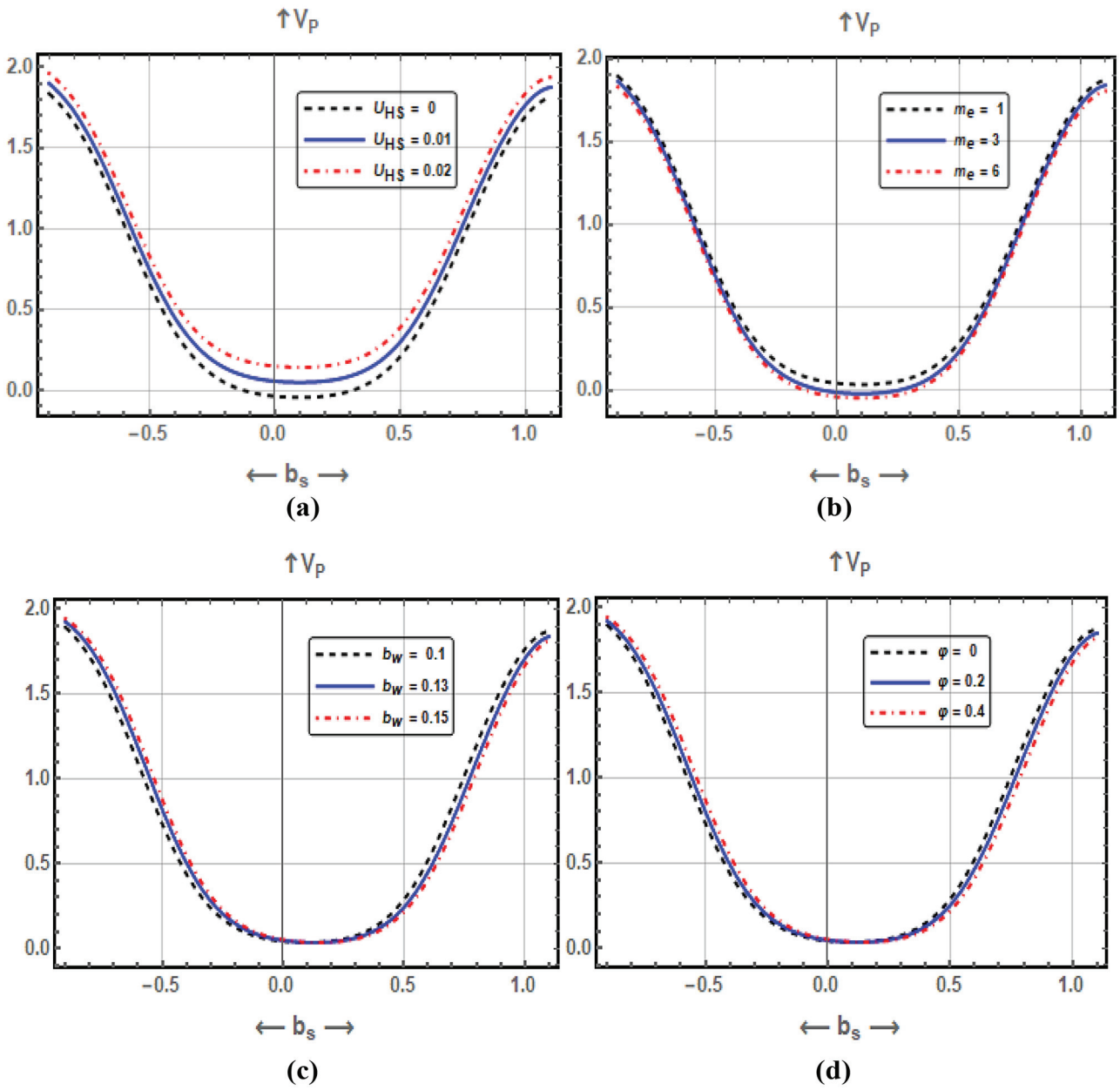

FIGURE 13. Plots for propulsive velocity *vs.* b_w for various values of U_{HS} (panel a); m_e (panel b); φ (panel c); b_w (panel d).

6.3. Pumping characteristics

Figures 12a–g illustrates the characteristics of pumping sperm into swimming plates along the basic direction of flow, which is an important and vital simulation of the transport of continuous sperm from the vagina to the uterus. As mentioned before, the pressure difference does not change above and below the swimming layers, it further investigated here with W_e, m_e, U_{HS}, φ and V_p. The pressure difference of the wavelength is divided into fourth significant quadrants. The first quadrant (where $P > 0$ and $Q > 0$) is known as the pumping of

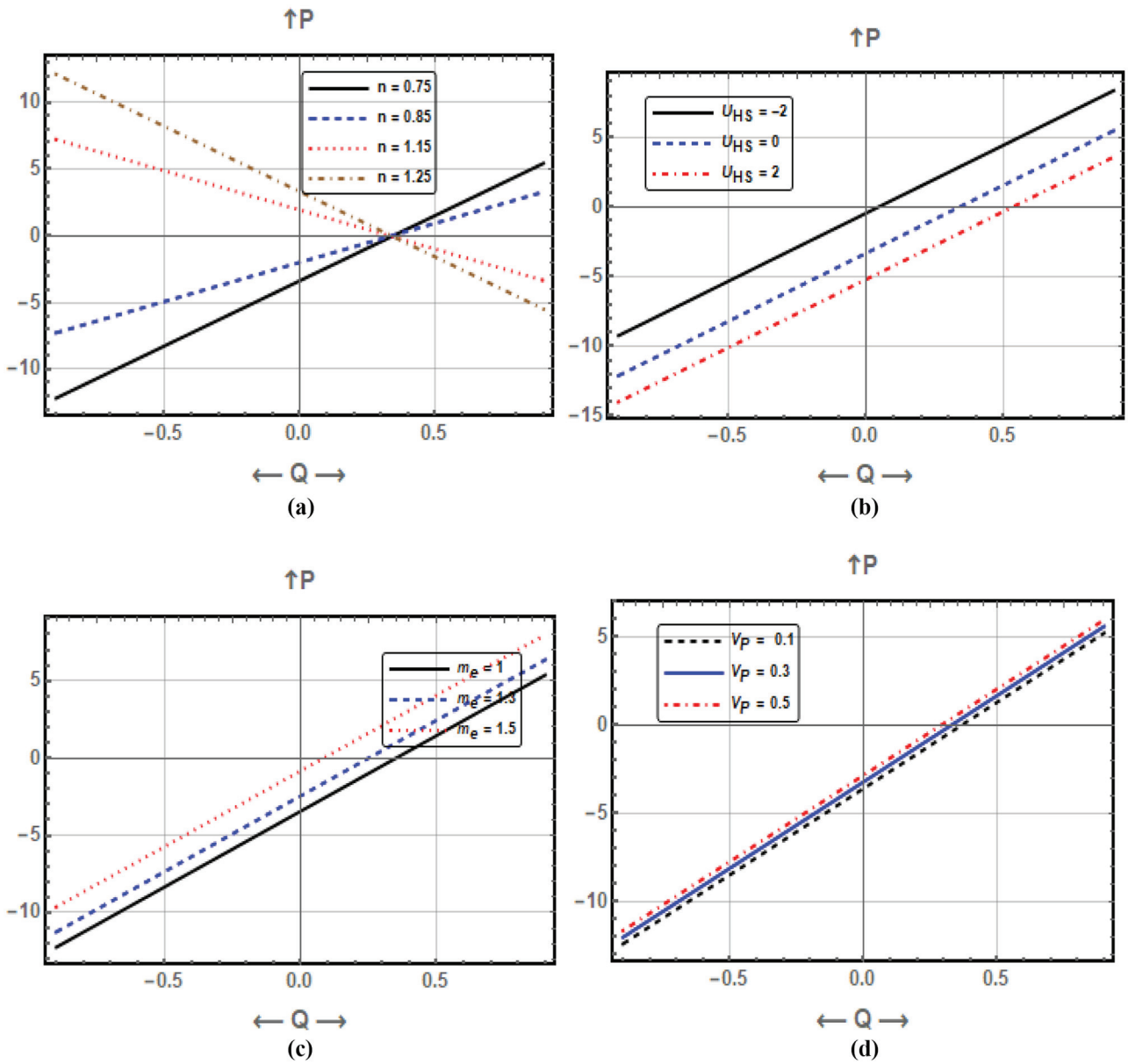

FIGURE 14. Plots for power delivered by the swimmer *vs.* Q for various values of n (panel a); U_{HS} (panel b); m_e (panel c); V_P (panel d).

the cervical sinusoidal area. The second quadrant ($P > 0$ and $Q < 0$) is known as the reverse pumping area through which flow occurs in the direction of the swimming layer of the sperm. The third quadrant ($P < 0$ and $Q < 0$) addresses a self-propelled pumping area where independent impulse waves dominate traveling and a pressure difference helps flow from the vagina to the uterus. Lastly, the fourth quadrant ($P < 0$ and $Q < 0$) addresses the increased pumping area where the pressure difference distinction enhances the stream. Figure 12a concludes that when W_e is increased, the pressure difference increases. Figure 12b deduces that the swimming sheet V_p enhances the pressure difference. Comparable behavior is noticed for Δp with U_{HS} as demonstrated in

Figure 12c. Figure 12d shows that the pressure difference diminishes with an increment in φ in the retrograde area after which the impact of φ starts to be changed in the cervical sinusoidal area before the pressure difference is seen to be incrementally changing in the augmented pumping area. Similarly, same behavior for the pressure difference is observed in Figure 12e when the wave amplitude b_s of microorganism sperm increases. Figure 12f reveals that the electroosmotic parameter reduces the pumping rate just as the behavior observed when n increases as shown in Figure 12g.

6.4. Propulsive velocity

Figure 13 describes the behavior of the propulsive speed of the swimming sheet versus the wave amplitude b_s of the microorganism sperm which relies upon φ, b_w, m_e, U_{HS} and Δp. It is noticed that U_{HS} has a decreasing effect on V_p as seen in Figure **13a**. A completely different pattern of activity has been seen from V_p with an enhancement in m_e as elucidated in Figure 13b. This means that in order to reduce or to maximize sperm velocity, it is better to enhance the Helmholtz-Smoluchowski velocity or apply an electroosmotic force in order to increase the sperm velocity. Consequently, the application of U_{HS} and m_e to the flow is remarkable in controlling sperm transport within the cervical canal. Figures 13c, d discloses that the demeanour of the propulsive velocity with wave amplitude b_w of the cervical wall and metachronal parameter where it is seen that an enhancement in V_p for the positive domain of the wave amplitude of the sperm, whereas and opposite effect occurs for a negative domain b_s.

6.5. Energy dissipation

Figure 14 discusses the energy dissipated (Power delivered by the swimmer) by the micro-organism computed using Mathematica Software verses flow rate Q for variation parameters rheological power law index (n), electroosmotic parameter $\boldsymbol{m_e}$, Helmholtz-Smoluchowski velocity $\boldsymbol{U_{HS}}$, and sperm speed. It is also seen that the rate of energy loss is an increasing function of the rheological power law index (n) as shown in Figure 14a, this implies that the surrounding fluid with shear-thinning nature leads to faster swimming with less energy consumption. As well, Figures **14b,c** shows that the energy dissipated decreases for increase of the Helmholtz-Smoluchowski velocity $\boldsymbol{U_{HS}}$ and increases when the electroosmotic parameter increases. This implies that the the electric double layer (EDL) region appears parallel to sperm fluid near to the cervical channel leads to faster swimming with less energy consumption. Also, it is clear that the energy dissipated increases for increase of the faster swimming as shown in Figure 14d.

7. Concluding remarks

The goal of this research is to look into the theoretical effects of electroosmotic forces on sperm swimming through the cervical canal. Sperm flow is caused by the peristaltic-ciliated wall that are centered on the walls with electroosmotic forces. Male semen with self-propulsive sperms is simulated by a hyperbolic tangent fluid. The biomechanics of the motility of swimming sperms is simulated mathematically using Navier Stoke's equations and using long-wavelength approximation. The governing equations are converted to ordinary differential system of equations and solved analytically to find mucus velocity, pressure difference, streamlines and propulsive velocity using Mathematica software program. The fundamental perceptions can be summed up as follows:

1. The rheological effect of hyperbolic tangent fluid is more appropriate to simulate and discuss the motility of cervical fluid.
2. The motility of mucus velocity is more applicable for small values of power law index at the upper swimming sheet of propulsive spermatozoa velocity.
3. The mucus velocity increases in the upper and lower region of swimming sheet with an enhancement in the electroosmotic parameter and Helmholtz-Smoluchowski velocity.
4. The metachronal parameter enhances the mucus velocity above and below the swimming sheet.
5. The mucus velocity attains the least values in the case of peristaltic flow field, while it continuously increases in the case of peristaltic ciliary flow.

6. The swimming sheet's propulsive velocity accelerates the mucus velocity through the upper and lower swimming sheet.
7. The Helmholtz-Smoluchowski velocity and the electroosmotic parameter are very important in controlling sperm transport within the cervical canal. This is supposed to help in the fertilization process.

Acknowledgements. Sara I. Abdelsalam expresses her deep gratitude to Fundación Mujeres por África for supporting this work through the fellowship awarded to her in 2020.

References

[1] S.I. Abdelsalam, Kh.S. Mekheimer and A.Z. Zaher, Alterations in blood stream by electroosmotic forces of hybrid nanofluid through diseased artery: aneurysmal/stenosed segment. *Chin. J. Phys.* **67** (2020) 314–329.

[2] S.I. Abdelsalam, J.X. Velasco-Hernández and A.Z. Zaher, Electromagnetically modulated self-propulsion of swimming sperms *via* cervical canal. *Biomech. Model. Mechanobiol.* (2021), DOI: 10.1007/s10237-020-01407-3.

[3] S.I. Abdelsalam, M.M. Bhatti, A. Zeeshan, A. Riaz and O.A. Bég, Metachronal propulsion of a magnetised particle-fluid suspension in a ciliated channel with heat and mass transfer. *Phys. Scr.* **94** (2019) 115301 [13 pages].

[4] Z. Asghar, N. Ali and M. Sajid, Analytical and numerical study of creeping flow generated by active spermatozoa bounded within a declined passive tract. *Eur. Phys. J. Plus* **134** (2019) 9.

[5] Z. Asghar, N. Ali, O. Anwar Bég and T. Javed, Rheological effects of micropolar slime on the gliding motility of bacteria with slip boundary condition. *Results Phys.* **9** (2018) 682–691.

[6] M.M. Bhatti, Biologically inspired intra-uterine nanofluid flow under the suspension of magnetized gold (Au) nanoparticles: applications in nanomedicine. *Inventions* **6** (2021) 28.

[7] M.M. Bhatti, A. Riaz, L. Zhang, S.M. Sait and R. Ellahi, Biologically inspired thermal transport on the rheology of Williamson hydromagnetic nanofluid flow with convection: an entropy analysis. *J. Therm. Anal. Calorim.* **144** (2021) 2187–2202.

[8] M.M. Bhatti, A. Zeeshan, M. Aleem Asif, R. Ellahi and S.M. Sait, Nonuniform pumping flow model for the couple stress particle-fluid under magnetic effects. *Chem. Eng. Commun.* (2021) DOI: 10.1080/00986445.2021.1940156.

[9] P. Gaddum-Rosse, R.J. Blandau and J.B. Thiersch, Ciliary activity in the human and *Macaca nemestrina* oviduct. *Am. J. Anatomy* **138** (1973) 269–275.

[10] S.K. Guha, H. Kaur and A.M. Ahmed, Mechanics of spermatic fluid transport in the vas deferens. *Med. Biolog. Eng.* **13** (1975) 518–522.

[11] P. Jyavel, R. Jhorar, D. Tripathi and M. Azese, Electroosmotic flow of pseudoplastic nanoliquids *via* peristaltic pumping. *J. Braz. Soc. Mech. Sci. Eng.* **61** (2019) 7–18.

[12] G. Li, E. Lauga and A.M. Ardekan, Microswimming in viscoelastic fluids. *J. Non-Newtonian Fluid Mech.* **297** (2021) 104655.

[13] D. Li and K. Li, Talk about several time periodic pulse electroosmotic flow of Maxwell fluid in a circular microchannel. *J. Appl. Math. Phys.* **9** (2021) 617–634.

[14] D. Lopez and E. Lauga, Dynamics of swimming bacteria at complex interfaces. *Phys. Fluids* **26** (2014) 071902.

[15] R.A. Lyons, E. Saridogan and O. Djahanbakhch, The reproductive significance of human Fallopian tube cilia. *Human Reproduct. Update* **12** (2006) 363–372.

[16] A. Mahdy and A. Hoshoudy, Two-phase mixed convection nanofluid flow of a dusty tangent hyperbolic past a nonlinearly stretching sheet. *J. Egypt. Math. Soc.* **27** (2019) 1–16.

[17] F.Y. Nakano, R.D.B.F. Leão and S.C. Esteves, Insights into the role of cervical mucus and vaginal pH in unexplained infertility. *Med. Express (São Paulo)* **2** (2015).

[18] G. Radhakrishnamacharya and R. Sharma, Motion of a self-propelling micro-organism in a channel under peristalsis: effects of viscosity variation. *Nonlinear Anal.: Modell. Control* **12** (2007) 409–418.

[19] K. Ramesh, A. Patel and M. Rawal, Electroosmosis and transverse magnetic effects on radiative tangent hyperbolic nanofluid flow through porous medium. *Int. J. Ambient Energy* (2021) 1–8.

[20] M. Rizwan, M. Hassan, O.D. Makinde, M.M. Bhatti and M. Marin, Rheological modeling of metallic oxide nanoparticles containing non-newtonian nanofluids and potential investigation of heat and mass flow characteristics. *Nanomaterials* **12** (2022) 1237.

[21] N. Saleem and S. Munawar, Entropy analysis in cilia driven pumping flow of hyperbolic tangent fluid with magnetic field effects. *Fluid Dyn. Res.* **52** (2020) 025503 [19 pages].

[22] S.S. Suarez and A.A. Pacey, Sperm transport in the female reproductive tract. *Human Reproduct. Update* **12** (2006) 23–37.

[23] S.S. Suarez, Mammalian sperm interactions with the female reproductive tract. *Cell Tissue Res.* **363** (2016) 185–194.

[24] A. Shahid, M.M. Bhatti, R. Ellah and Kh.S. Mekheimer, Numerical experiment to examine activation energy and bi-convection Carreau nanofluid flow on an upper paraboloid porous surface: application in solar energy. *Sustain. Energy Technolog. Assess.* **52** (2022) 102029.

[25] A. Tanveer, S. Mahmood, T. Hayat and A. Alsaedi, On electroosmosis in peristaltic activity of MHD non-Newtonian fluid. *Alexandria Eng. J.* **60** (2021) 3369–3377.

[26] A. Walait, A.M. Siddiqui and M.A. Rana, Mathematical assessment of the spermatozoa transport through couple stress fluid in an asymmetric human cervical canal. *Theory Biosci.* **139** (2020) 235–251.

[27] L. Zhu, E. Lauga and L. Brandt, Low-Reynolds-number swimming in a capillary tube. *J. Fluid Mech.* **726** (2013) 285–311.